INTERNATIONAL JOURNAL FOR NUMERICAL AND ANALYTICAL METHODS IN GEOMECHANICS
Int. J. Numer. Anal. Meth. Geomech., **23**, 1977–1994 (1999)

SIMULATION OF GEOMEMBRANE RESPONSE TO SETTLEMENT IN LANDFILLS BY USING THE MATERIAL POINT METHOD

SHIJIAN ZHOU[1], JOHN STORMONT[2] AND ZHEN CHEN[3,*]

[1]*GM Advanced Technology Vehicles, 9900 Westpoint Dr., Suite 142, Indianapolis, IN 46256, U.S.A.*
[2]*Department of Civil Engineering, University of New Mexico, Albuquerque, NM 87131, USA*
[3]*Department of Civil and Environmental Engineering, University of Missouri, Columbia, MO 65211, USA*

SUMMARY

Because of the multiple layers of dissimilar materials and large deformations involved in the subsidence of a landfill system, large-scale computer simulation of the geomechanical response to subsidence with the use of conventional numerical methods are problematic. The Material Point (MPM),[1,2] which was recently developed for dynamic problems such as penetration and perforation, is a newly emerging numerical method. The MPM is modified in this paper to simulate the geomechanical response of a landfill cover system that includes a geomembrane under quasi-static loading conditions. Sample problems, for which an analytical solution is available with certain assumptions, are considered to demonstrate the proposed solution procedure. Future work is discussed based on current research results. Copyright © 1999 John Wiley & Sons, Ltd.

KEY WORDS: geomembrane; subsidence; landfill; large deformations; material point; simulation

1. INTRODUCTION

The degradation and creep of the contents of a landfill will cause the surface to subside. The amount of subsidence can be very large, on the order of 25 per cent or more of the original height of the waste.[3] These large deformations cause a number of deletrious effects on the surface cover system. The surface cover, an engineered system comprised layers of soils and synthetic materials, is principally designed to limit water movement into the underlying waste. A principal concern regarding subsidence is its affect on low-permeability barrier layers within the cover system. Compacted soil layers have historically been a common barrier layer component of many landfill covers. Compacted soil layers are susceptible to tension cracking and multiple shear rupturing in response to subsidence (e.g. References 4 and 5), resulting in dramatic increases in their hydraulic conductivity. Many newer landfill cover systems now incorporate geomembranes (e.g. high-density polyethylene) which are often placed on the top of a compacted soil layer to form a composite barrier to infiltration of water through the cover system. An attribute of geomembranes in contrast to compacted soil layers is that they can withstand large tensile

*Correspondence to: Dr. Z. Chen, Department of Civil and Environmental Engineering, University of Missouri-Columbia, E2059 Engineering Building East, Columbia, MO 65211-2200, USA.

CCC 0363–9061/99/151977–18$17.50

Received 15 July 1998
Revised 5 March 1999

strains corresponding to large differential settlements (e.g. Reference 6). Oweis[7] suggested that geomembrane may be able to support differential settlements well in excess of 10 per cent.

Due to the highly nonlinear response, numerical simulations are commonly used to predict the impact of subsidence on the integrity of a landfill cover. The finite element method has been used in many cases (e.g. References 8 and 9). Simulating subsidence of a landfill cover that includes a geomembrane is challenging for existing numerical methods as the cover includes multiple layers of dissimilar materials experiencing very large absolute and relative deformations. To accommodate the expected differential movement between the soil layers and the geosynthetic layers, interface elements are usually used to simulate a frictional interface. To obtain reasonable results, fine discretization is required in the vicinity of the subsided zone, resulting in a huge degrees of freedom. Additionally, the numerical formulation must be capable of simulating the large strains anticipated for these subsidence problems. When localization occurs, a robust spatial discretization scheme is needed to simulate the evolution of localization with least computational cost.

The Material Point Method is a newly emerging numerical method which may by effective for simulating certain geomechanical problems such as the response of a landfill cover system that involves a geomembrane to subsidence. The MPM utilizes two different elements: material elements (or points) and spatial elements. Material points carry all of the material specific information such as mass, strain, velocity, acceleration, energy, and internal state variables. These variables are updated as Lagrangian quantities which ensures that this approach has little numerical dissipation. A fixed Eulerian grid which comprised spatial elements is used to determine spatial gradients. Since the spatial grid is independent of the movement and deformation of the material, there is no mesh entanglement and no need to update the grid. The MPM has successfully been applied to those problems such as penetration, impact and large rotation of solid bodies,[1,2,10] but has not yet been applied to geotechnical problems under quasi-static loading conditions.

In this paper, the MPM is applied to the problem of subsidence of landfill covers that include geomembranes. A brief description of the MPM is given first, followed by a description of modifications and additions necessary to simulate the subsidence problem. An example problem is presented to compare simplified analytical solutions with the numerical results using the MPM. The paper concludes with a discussion and summary of the use of the MPM for geotechnical problems.

2. MATERIAL POINT METHOD

The Material Point Method (MPM) is an extension of the particle-in-cell method in solid mechanics. This method has initially been developed for and successfully applied to problems with large deformations, large rotations, and large displacements such as collision, rebound, and impact of solids; penetration, perforation, and crack propagation; forging, extrusion, metal rolling, and cutting; and fluid–structure interaction. Since there are large deformations, rotations, and displacements associated with landfills, the MPM may be an appropriate numerical method for simulating the structural response of materials in and surrounding landfills. This section provides a brief description on the MPM and its numerical implementations in which key points that distinguish this approach from others are emphasized. A detailed description and discussion of the MPM can be found in References 1 and 2.

2.1. Introduction of the material point method

In the 1960s, the particle-in-cell method (PIC)[11] was introduced for describing a highly distorted flow. The method is able to resolve a contact discontinuity because of the Lagrangian representation of mass so that details of the deformation and movement of a body can be followed during the entire loading process. PIC was not widely used because of its unacceptable numerical dissipation caused by its partial Lagrangian scheme in that only mass and position are attributed to each particle.

FLIP[12] is a fully Lagrangian implicit particle method for fluid flow. It improved PIC with the use of a fully Lagrangian representation which eliminates the major source of numerical dissipation while preserving the ability to resolve a contact discontinuity. Burgess *et al.*[13] show that FLIP attributes all of the properties, including momentum and energy of a fluid, to material points so that diffusion of these variables is eliminated just as mass diffusion is eliminated in PIC by making the mass a Lagrangian variable. To eliminate the multistreaming, FLIP calculates the material point displacement by interpolating from the grid velocity field. FLIP has been shown to have several desirable advantages, among them Galilean invariance, low dissipation, conservation of momentum and energy, and improved stability over the earlier PIC method. These properties make FLIP an effective procedure for simulating a highly distorted fluid flow and resolving contact discontinuity in a wide range of problems, including hydrodynamic stability, suspension flows,[14] strength of material problems, chemically reacting flows, and magnetic reconnection.

Sulsky *et al.*[15,16] first extended FLIP to solid mechanics where it is referred to the material point method or MPM for materials associated with history-dependent state variables. Recently, the MPM has been used to analyse the large deformation problems of history-dependent materials,[1,2] which circumvents some of the major obstacles encountered in the pure Lagrangian or Eulerian methods, and traditional arbitrary Lagrangian and Eulerian methods.

2.2. Numerical implementation

As shown in Figure 1, two different and independent elements are introduced in the MPM to take advantage of both Eulerian and Lagrangian features: spatial elements represented by rectangles, and material elements by dotted polygons identified with material points (solid circles). Material points represent different materials and carry all the information such as mass, strain, stress, velocity, acceleration, momentum, and energy. All these variables are updated as Lagrangian quantities which ensures that this approach has little numerical dissipation. The computational grid is constructed of spatial elements which are used to determine spatial gradients and to interpret the interaction between material points using a finite element framework. Since the spatial grid is independent of the movement and deformation of the material, there is no mesh entanglement and no need to update the grid. Additionally, since all the material points are tracked for the entire loading process, the MPM can simulate path-dependent responses without introducing errors. The convective phase of this method is carried out by the movement between material points and computational grid.

The complete algorithm consists of the following steps: (1) a Lagrangian phase where the equations of motion are solved in an updated Lagrangian frame on the grid; (2) a convective phase where the particles are updated and the grid is redefined; (3) a transformation process in

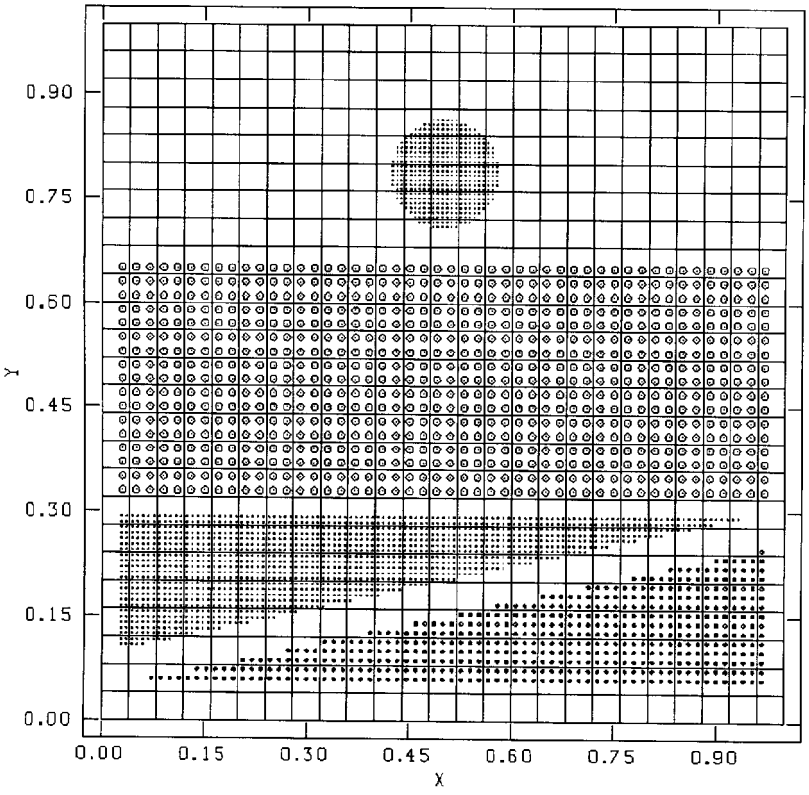

Figure 1. MPM method

which the information is mapped from the material points to a grid. These three steps are described briefly as follows.

In the MPM, the discrete momentum equation associated with the node is solved on the spatial grid:

$$m_i \mathbf{A}_i = \mathbf{F}_i^{\text{int}} + \mathbf{F}_i^{\text{ext}} \tag{1}$$

in which m_i is a lumped mass on the ith node, $\mathbf{A}_i$ the acceleration vector, and $\mathbf{F}_i^{\text{int}}$ and $\mathbf{F}_i^{\text{ext}}$ internal and external force vectors, respectively. The solution in a Lagrangian frame means that the non-linear convective terms, that are troublesome in purely Eulerian calculations, do not appear in the formulation. Once the accelerations at the grid nodes are determined, an explicit time integration gives values for the nodal velocity vector, $\mathbf{V}_i$, as follows:

$$\mathbf{V}_i = \mathbf{V}_i + \Delta t \mathbf{A}_i \tag{2}$$

where Δt is the time increment, i.e. $\Delta t = t^k - t^{k-1}$. The nodal position vector, $\mathbf{X}_i$, is given by

$$\mathbf{X}_i = \mathbf{X}_i + \Delta t \mathbf{V}_i \tag{3}$$

The convection phase is performed by moving material points along with the grid and fixing them at the new position while shifting the computational grid back to its original position.

During the entire calculation cycle, however, equation (3) is never used since the computational grid always keeps the same shape at the same position for convenience. Velocities and positions of material points can be updated by

$$\mathbf{V}_p = \mathbf{V}_p + \Delta t \sum_{i=1}^{N} \mathbf{A}_i S_{pi} \tag{4}$$

and

$$\mathbf{X}_p = \mathbf{X}_p + \Delta t \sum_{i=1}^{N} \mathbf{V}_i S_{pi} \tag{5}$$

in which S_{pi} is the mapping function associated with the ith node and evaluated at the position $\mathbf{X}_p$, and N is the number of nodes associated with that material point. Strain rate at a material point, $\dot{\varepsilon}_p$, can be calculated based on its velocity gradients, and the corresponding stress rate, $\dot{\sigma}_p$, can be obtained by applying constitutive equations to that material point. The total stress at the material point can be updated by

$$\sigma_p = \sigma_p + \Delta t \dot{\sigma}_p \tag{6}$$

In order to solve the discrete momentum equation for next time step, information must be transferred from the material points to the grid nodes. The equation to obtain the nodal mass from material points is

$$m_i = \sum_{p=1}^{N_p} m_p S_{pi} \tag{7}$$

in which N_p is the number of material points associated with that grid node. Since there are generally more material points than grid nodes, a weighted least-squares approach is used to determine nodal velocities from the velocities at the material points to initialize next time step. The weighting factor is the mass of the material point. The result is the following equation which must be solved for the nodal velocities, $\mathbf{V}_i$,

$$m_i \mathbf{V}_i = \sum_{p=1}^{N_p} m_p \mathbf{V}_p S_{pi} \tag{8}$$

The internal force can be formed by

$$\mathbf{F}_i^{\text{int}} = \sum_{p=1}^{N_p} m_p (\mathbf{G}_{ip}^{\mathrm{T}} \cdot \sigma_p^{\mathrm{s}}) \tag{9}$$

in which $\mathbf{G}_{ip}^{\mathrm{T}}$ is the gradient of mapping function associated with the ith node and evaluated at the material point position $\mathbf{X}_p$. This completes the computational cycle. With the use of these updated nodal values at the grid, a new cycle can begin.

In comparison with traditional finite element methods, the MPM has the following essential features:

(1) When the material points move, they transport material properties assigned to them without error. The grid has no permanent information and can be chosen in any convenient manner, for example, adaptive grids can be used to resolve sharp gradients or interfaces. A particularly simple choice is the regular square mesh that is used in our numerical examples.

(2) Since nodal basis functions are used to map the nodal velocity continuously to the interior of the spatial element, the position of the material points are updated by moving them in a single-valued, continuous velocity field. Similarly, the velocity of a material point is updated by mapping the nodal accelerations to the material point position. The single-valued velocity field precludes interpenetration of material. This feature of the algorithm allows simulation of landfill problems with multiple layers with widely different properties without the need for a special contact algorithm.

3. MODIFICATIONS TO THE MPM

3.1. Partition method

The MPM is based on a dynamic framework. For quasi-static problems, a significant unbalanced force field appear when material points cross spatial cell boundaries.[10] Thus a modification to the MPM is needed for quasi-static problems.

Consider the two-dimensional problem shown in Figure 2. An elastic bar is fixed at one end and uniaxial loading is applied quasi-statically at its free end. Figure 2(a) shows the initial configuration and Figure 2(b) is the deformed configuration where two material points have crossed the cell boundary. There is no external force at the internal node i if the gravity force is ignored. The internal force at that node should be zero at the equilibrium state, and can be calculated by equation (9).

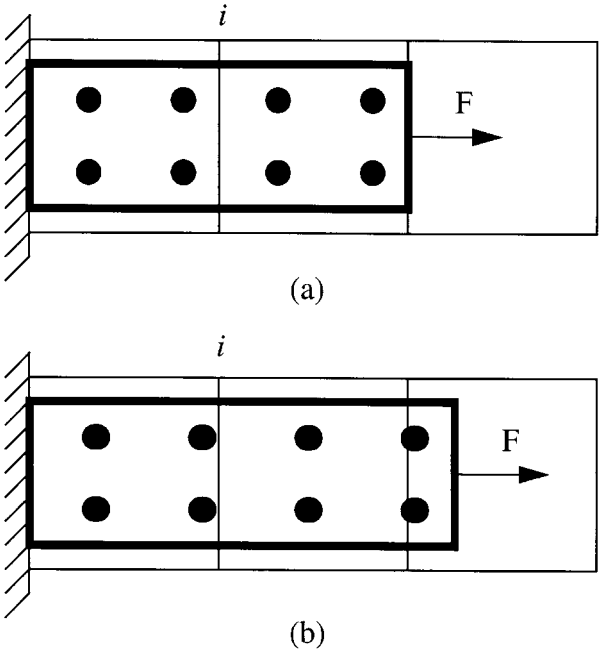

Figure 2. An elastic bar under uniaxial loading

If the summation is performed in the manner of sweeping over element by element, equation (9) can be written as

$$F_i^{\text{int}} = -\sum_{c=1}^{N_c}\sum_{pc=1}^{N_{pc}} m_{pc}(G_{ipc}^{\text{T}}\sigma_{pc}^{\text{s}}) \tag{10}$$

in which the subscript denotes that a quantity is related to a cell. For an incompressible material and with unified mass setting for each material point, m_{pc} is a constant. Under the assumption of equilibrium in an elastic calculation, σ_{pc}^{s} is also a constant so that equation (10) becomes

$$F_i^{\text{int}} = -m_{pc}\sigma_{pc}^{\text{s}}\sum_{c=1}^{N_c}\sum_{pc=1}^{N_{pc}} G_{ipc}^{\text{T}} \tag{11}$$

By using a bilinear mapping function, the value of its gradient at a grid node will be independent of the material point position in an element and may change its sign in another element. For a symmetric problem under a uniaxial loading the above equation reduces to

$$F_i^{\text{int}} = -m_{pc}\sigma_{pc}^{\text{s}}c(N_{\text{l}} - N_{\text{r}}) \tag{12}$$

where N_{l} and N_{r} are the number of material points in the left and right cell and c is the constant associated with gradients. This result shows that the force field at the interior of the bar is zero initially and it maintains zero under a static loading process until material points cross the cell boundary (Figure 2). With a perfect square material point generation algorithm and under a uniaxial loading, the difference, $N_{\text{l}} - N_{\text{r}}$, should be the square root of the number of material points per cell, $\sqrt{N_c}$. Expressing the mass in terms of density, ρ_{pc}, volume, V, and N_c, equation (12) can be written as

$$F_i^{\text{int}} = -\frac{c\rho_{pc}V\sigma_{pc}^{\text{s}}}{\sqrt{(N_c)}} \Rightarrow \lim_{N_c \to \infty} F_i \to 0 \tag{13}$$

Equation (13) can be also used as an absolute error measure since the internal force should be zero for a static calculation. It also indicates that the solution will be improved with increasing the number of material points per cell. Practically, a partition MPM algorithm (PMPM) proposed in this paper views a material point as a finite continuum when it crosses a cell boundary. In PMPM, a material point maintains the original undeformed shape during its entire deformation history. This treatment makes boundary crossing process in a gradual manner instead of a suddenly movement from one cell to the another. The following figure illustrates different cases of boundary crossing and the arrows show how a quantity is mapped from split material points to grid nodes. With this modification, the internal force and mass calculations at grid nodes take following forms (derivations are given in Appendix I):

$$F_i^{\text{int}} = -\sum_{q=1}^{N_q}\sum_{p=1}^{N_p} m_{pq}(G_{ipq}^{\text{T}}\sigma_{pq}^{\text{s}})S_{ipq} \tag{14}$$

and

$$m_{ij} = -\sum_{q=1}^{N_q}\sum_{p=1}^{N_p} m_{pq}(S_{ipq}^{\text{T}}\,S_{pqj}) \tag{15}$$

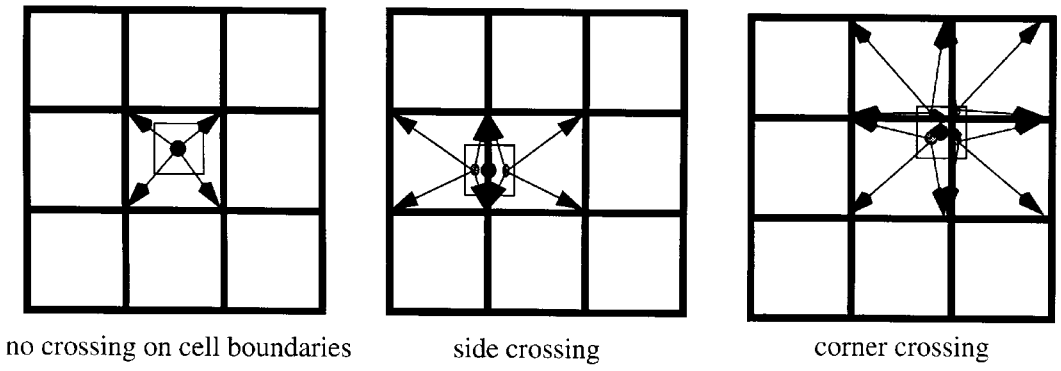

Figure 3. Illustration of different boundary crossing cases

For the problem, illustrated in Figure 2, the internal force can be written as follows:

$$F_i^{\text{int}} = -\sum_{c=1}^{N_c}\sum_{q=1}^{N_q}\sum_{p=1}^{N_p} m_{pqc}(G_{ipqc}^{\text{T}}\sigma_{pqc}^{\text{s}})S_{ipqc} \tag{16}$$

then, the assumptions of incompressible material, equilibrium state and elastic calculation give

$$F_i^{\text{int}} = -\sigma^{\text{s}}(m_{\text{cl}} - m_{\text{cr}}) \tag{17}$$

where

$$m_{c_1} = \sum_{q=1}^{N_q}\sum_{p=1}^{N_p} m_{pqc_1} S_{ipqc_1} \quad m_{c_r} = \sum_{q=1}^{N_q}\sum_{p=1}^{N_p} m_{pqc_r} S_{ipqc_r} \tag{18}$$

in which C_1 and C_r denote the left spatial element and right spatial element, respectively. For small deformations, the summations of mass on a grid node in equation (18) are the same, i.e., $m_{c_1} = m_{c_r}$. This leads to existence of the following limit with refining a mesh:

$$\lim_{N_e \to \infty} F_i \to 0 \tag{19}$$

where N_e is the number of spatial elements. The corresponding strain expression is as follows (its derivation is given in Appendix II):

$$\varepsilon_{pq} = \sum_{i=1}^{N} \mathbf{V}_i \otimes \mathbf{G}_{ipq}^{\text{T}} S_{ipq} \tag{20}$$

The equations given in this section are similar in form to those given in Section 2 but with some important differences in both physical concept and numerical results. In PMPM, the cell mass, m_c, which is the summation of total mass in a cell is almost unchanged. It effectively removes the jump in both force and velocity fields when a material point crosses a cell boundary. The numerical algorithm is basically the same as the one discussed in Section 2 except using equations 14, 15 and 20 to calculate the internal force, mass, and strain.

3.2. *Interface algorithm*

The MPM provides a natural no-slip and no-interpenetration contact algorithm. For many geomechanical problems, frictional interfaces are required. Landfill covers, for example, typically have a number of discrete frictional interfaces such as geomembranes and adjacent soils. A friction interface algorithm is proposed in this paper that provides an easy way to change the boundary conditions of interfaces such as soil–geomembrane contact surfaces or interfaces. With a geomembrane, slip is possible on both its upper and lower surfaces. No-slip and free-slip are extreme conditions of friction. No-slip is perfect friction where a material layer adheres to another material layer. Free-slip represents zero friction where the tangential motion of one material is not affected by the other. Interface modelling is often a cumbersome task in finite element codes. In contrast, the MPM provides a readily accessible framework to model interface boundaries. In the MPM, a no-interpenetration boundary condition is accomplished by moving material points in an unified velocity field. Since interpenetration has nothing to do with the tangential velocity but friction force does on the interfaces, we can convert the friction force into tangential velocity field and allow certain slip between different material layers according to the friction criterion applied on the interface. In the meantime, the normal velocity field remains the same for all different material layers. To implement the algorithm, it is necessary to find the unit normal to the interface surfaces and at its external grid nodes, find the normal velocity and tangential velocity on the interfaces, and keep the normal velocity unchanged and modify the tangential velocity to meet the friction boundary conditions at external grid nodes.

The appropriate grid nodes at which to apply the friction interface boundary conditions are determined with the deformation history during the MPM calculation. To simplify the determinations of the nearest external grid nodes and the tangential and normal directions at those nodes, a single layer of material points was used to represent a geomembrane layer. It is easy to label external nodes by sweeping the single layer material points. The unit tangential and normal vectors can be determined based on the position vectors of the adjacent material points. The tangential and normal directions on the upper and lower interfaces of the geomembrane are in the opposite direction. The effect of the friction conditions was modelled by adjusting the force field at the selected external grid nodes.

To allow more complexity of the deformed shape of a geomembrane, a general scheme of determining external grid nodes and outward surface unit normal are proposed by Reference 2. The scheme begins by tagging material points comprising the geomembrane with a 'colour' of one, while the material points comprising other materials are given a 'colour' of zero. Only the non-zero color will contribute to selection of external grid points and unit normal. The colour of each material points in a cell is summed up and the number of points in each cell is also summed. Every points is counted independently of its assigned colour. The total colour of the cell is then divided by the number of points in that cell, allowing for 'mixed' cells containing points from multiple materials where some points contribute to the total colour and others do not. Cells containing points from multiple materials have an average colour of less than one. The average colour is understood to be assigned at the centre of the cell. A mapping of the gradient of the average colour is made from the centre of the cell to the cell grid nodes. The gradient mapping scheme is equivalent to finding a central difference of the average colour between the centre of each cell in the x- as well as in the y-direction. The x and y components of the gradient of colour are zero at grid nodes internal to the material where no gradient exists, and non-zero at grid nodes in a surface region external to a material where gradients of colour do exist. All the grid

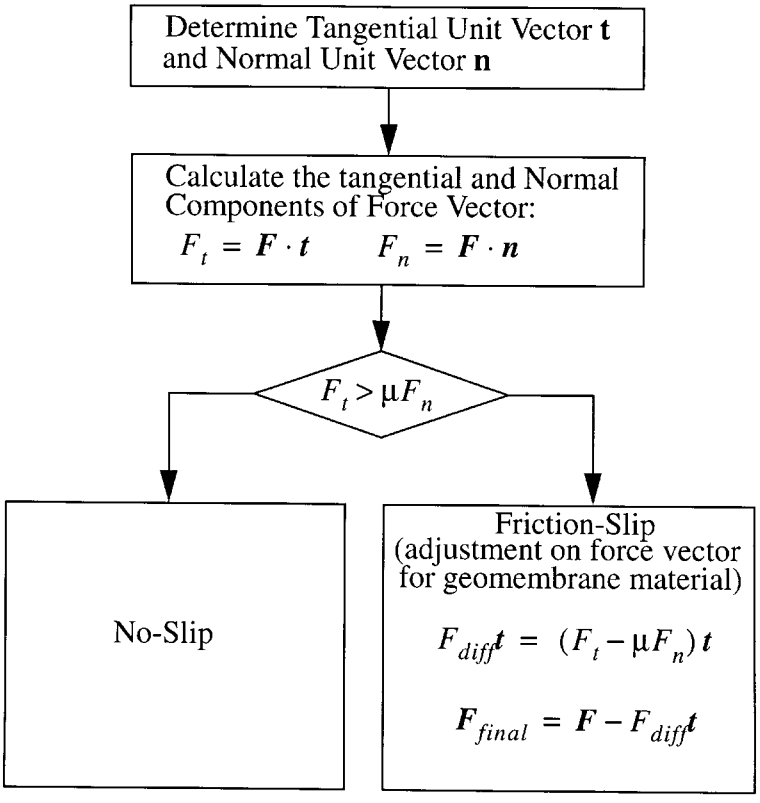

Figure 4. Flow diagram for Coulomb friction-slip cover subsidence algorithm

nodes associated with non-zero normal are tagged as the external grid nodes where Coulomb friction-slip is enforced to establish the desired interface between materials.

The algorithmic representation of Coulomb friction-slip enforces interface conditions on both the forces and velocities at selected external grid nodes on the geomembrane interfaces. To illustrate the logic of a Coulomb friction-slip contact algorithm, the interface conditions of Coulomb friction-slip in terms of force field are shown as a flow diagram in Figure 4, in which F_{diff} is the adjustment on tangential force component, $\mathbf{F}$ and $\mathbf{F}_{\text{final}}$ are the total force before and after adjustment, respectively. This approach is difficult to be implemented since there is no force field directly related to the material points in a MPM calculation. The key to implement the interface algorithm is to work with the velocity variables at the material points rather than the force field variables at the spatial nodes, thus avoiding inconsistent friction conditions at different associated grid nodes for a interface material point. The flow diagram of the modified algorithm representation is shown in Figure 5. The formulations in velocity form are obtained by simply applying $\mathbf{F}\Delta t = \Delta \mathbf{V}m$ to the one in force form.

The friction velocity is defined as the normal velocity times a friction factor, μV_n. Having obtained the tangential and normal velocities, the modified algorithm tests for velocity at a interface material point by whether or not the tangential velocity on the interface under the

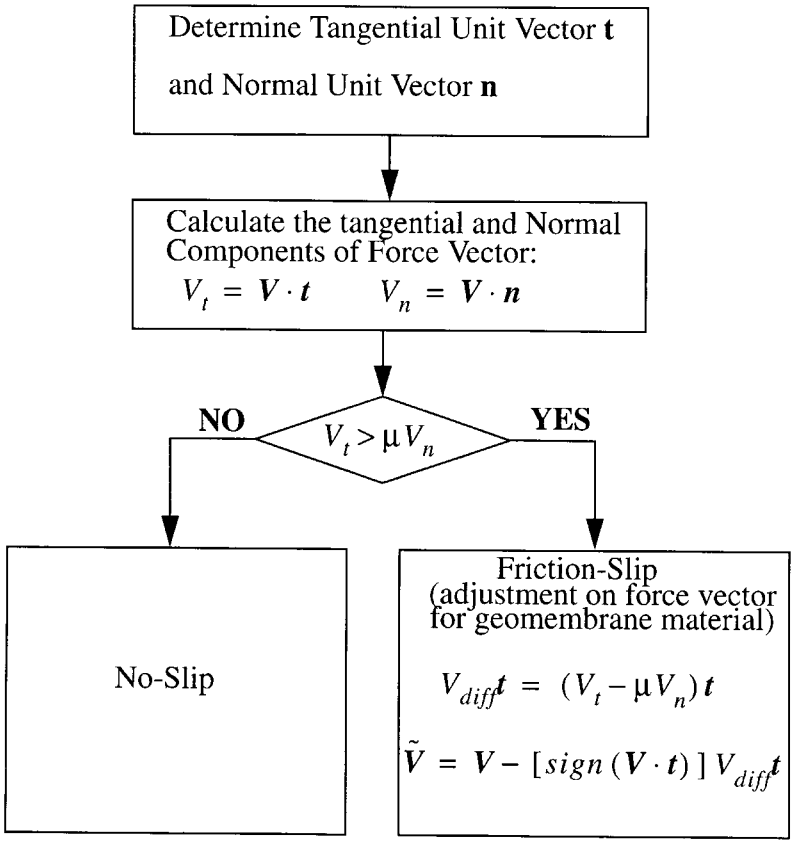

Figure 5. Flow diagram for modified algorithm

assumption of no-slip condition is greater than the friction velocity. If this condition fails, interface treatment is not active, assuming that the friction force on the interface material point has not increased to a sufficient value to cause friction-slip. If the condition is satisfied, the algorithm will adjust the velocity to be consistent with the slippage associated with friction force by subtracting the difference between the no-slip tangential velocity and the friction velocity. A sign function is employed for when the inner product of the velocity and tangential is greater or less than zero. Slippage occurs because adhering to adjacent material is not enforced by permitting the geomembrane to have a tangential velocity that differs from that of the adjacent material. No-interpenetration is retained since the normal velocity of a interface material point remains the same.

4. ANALYSIS OF GEOMEMBRANE RESPONSE TO LANDFILL SUBSIDENCE

In this section, an example problem is considered to simulate the subsidence of a landfill cover. The landfill cover consists of a cover soil overlying a geomembrane and the waste underneath. The simplicity of the design belies the complicated behaviour that occurs due to the differences in

material properties between the soil and the geomembrane. If possible, it is useful to compare the simulation results to an analytical solution. With certain assumptions, an analytical solution exists for the stress and strain in a geomembrane that develops in a soil–geomembrane system overlying a void. Thus, the numerical simulations will focus on the stress and strain that develop in a geomembrane in response to subsidence from below, in order to compare them to an analytical solution.

4.1. Numerical simulations

The problem configuration is shown in Figure 6. To demonstrate the proposed procedure, the height of the soil, geomembrane and waste are 8, 1 and 30 mm, respectively. To induce subsidence, a very soft material of 6 mm diameter is introduced immediately below the geomembrane. Because the cover soil is essentially just a load to this boundary value problem, a soil density is chosen for the current soil dimension so that the resulting soil unit weight on the geomembrane is the same as that in the real cases. We apply different soil unit weights by simply changing soil densities as shown in Table I. The external load on the geomembrane is due to the soil weight in this quasi-static case. Soils and waste are modelled as Drucker–Prager elastoplastic materials, and the geomembrane is assumed to be von Mises elastoplastic. To compare numerical solutions with analytical solutions, only the elastic response is considered here with elastic properties and unit weights for the materials being given in Table I, and perfect bonding is assumed between different material layers so no friction occurs along the interface.

The simulated deformations for load I are shown in Figure 7. At the centre of the subsided zone, the geomembrane deforms 1 mm. For load II, the maximum geomembrane deformation

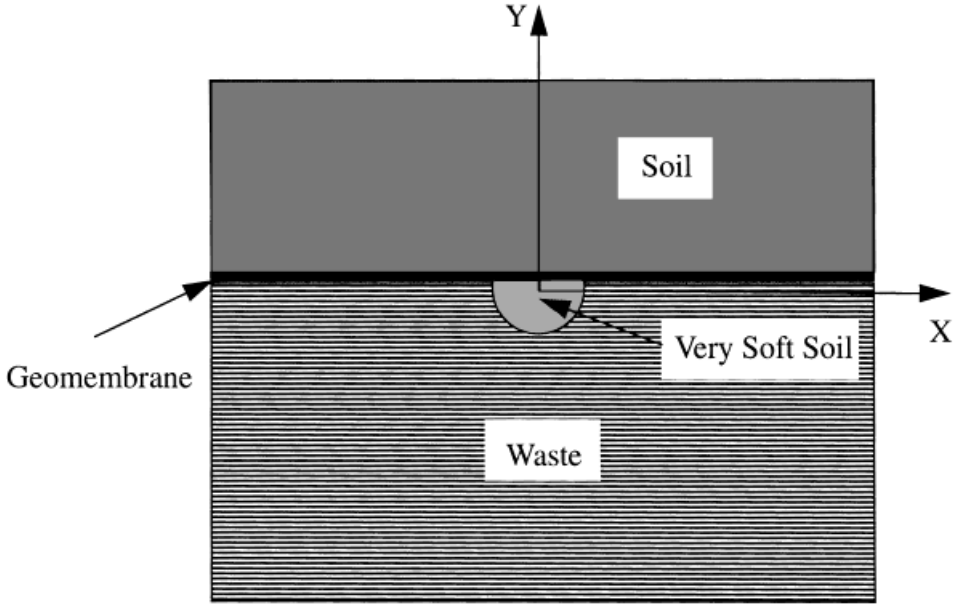

Figure 6. Geometry of a landfill problem

Table I. Material properties

	Young's modulus (GPa)	Poisson's ratio	Unit weight I (kg/m^3)	Unit weight II (kg/m^3)
Soil	0·1317	0·25	7,500,000,000	1,500,000,000
Geomembrane	0·2070	0·40	5,000,000	9,550,000
Waste	0·1317	0·20	1,000,000	2,000,000
Soft material	0·0034	0·30	1,000	2,000

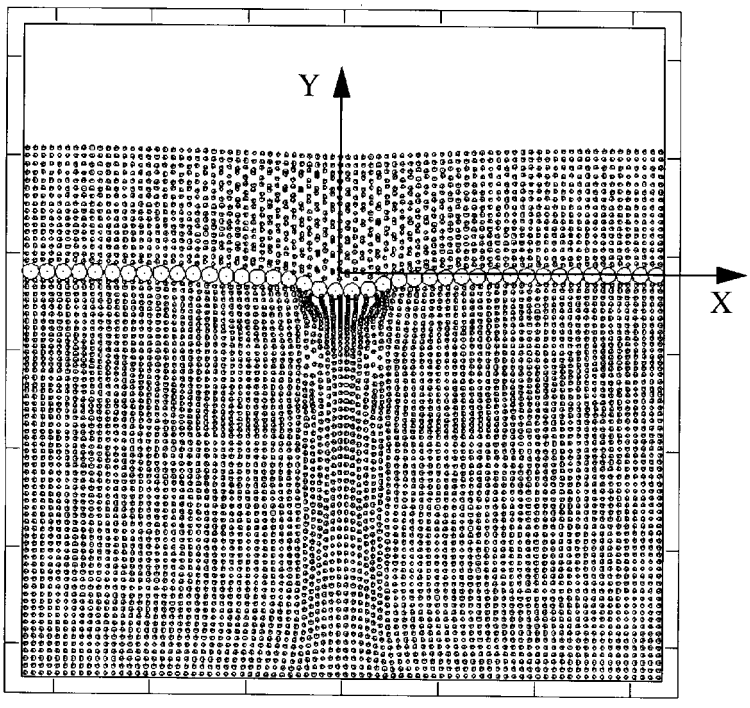

Figure 7. Deformation contour plot

increases to 2 mm. The geomembrane deforms outside the boundary of the subsided zone, as does the overlying soil. In Figure 8, the axial strain in the geomembrane is given with the centre of soft material (6 mm diameter) being at $X = 15$ mm, revealing a maximum axial strain of about 6 and 12 per cent for the load levels I and II, respectively. The strain level dissipates rapidly because the strain is transferred rapidly across the interface from the geomembrane to the adjacent relatively stiff soil.

It is interesting to compare the results from the simulations with an analytical solution for the stress and strain that develops in a geomembrane which overlies a void.[17] The void is intended to represent sinkholes, cavities, and depressions in soils due to differential settlements or localized

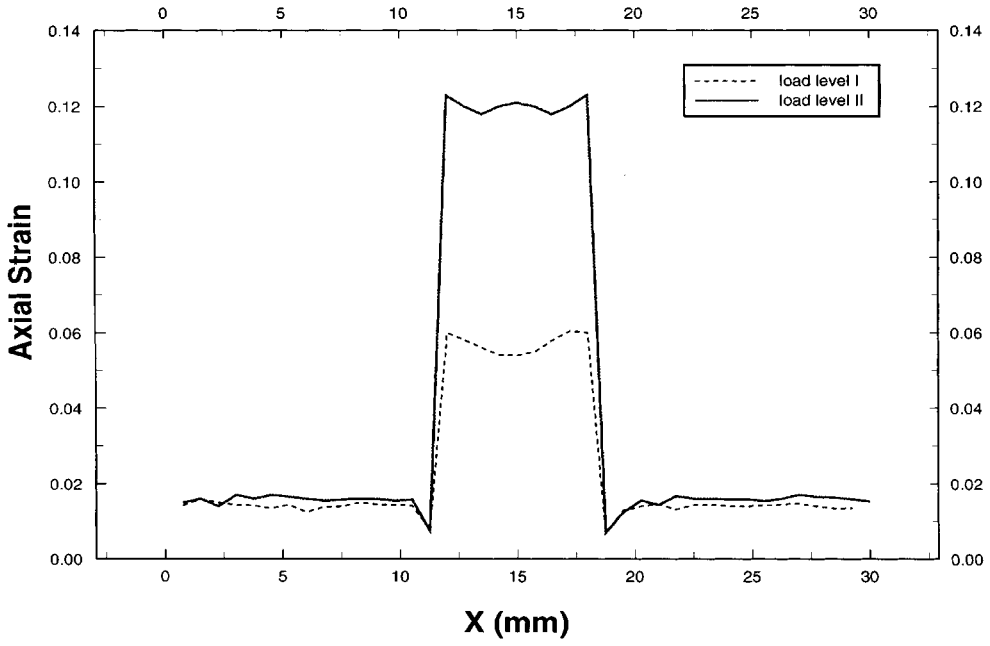

Figure 8. Axial strain in geomembrane

subsidence. The solution was developed by combining tensioned membrane theory for the geomembrane with arching theory for the overlying soil. Arching theory is first used to calculate the pressure p on the geomembrane over the void, which yields

$$p = 2\gamma b(1 - e^{0\cdot5\times H/b}) + qe^{-0\cdot5\times H/b} \tag{21}$$

where γ is the unit weight of the soil, b is the width of the void, H is the height of the overlying soil, and q is a surface load. This equation assumes a constant lateral earth pressure in the soil zone where the arching develops. Tensioned membrane theory is used to determine the stress and strain of the geomembrane due to the pressure from the overlying soil. The axial stress σ in the geomembrane is given by

$$\sigma = \frac{pb\Omega}{t} \tag{22}$$

where t is the thickness of the geomembrane and Ω is a dimensionless factor defined by

$$\Omega = \frac{1}{4}\times\left(\frac{2y}{b} + \frac{b}{2y}\right) \tag{23}$$

where y is the deformation of the geomembrane over the middle of the void. The strain ε in the geomembrane is

$$\varepsilon = 2\Omega \sin^{-1}\left(\frac{1}{2\Omega}\right) - 1 \tag{24}$$

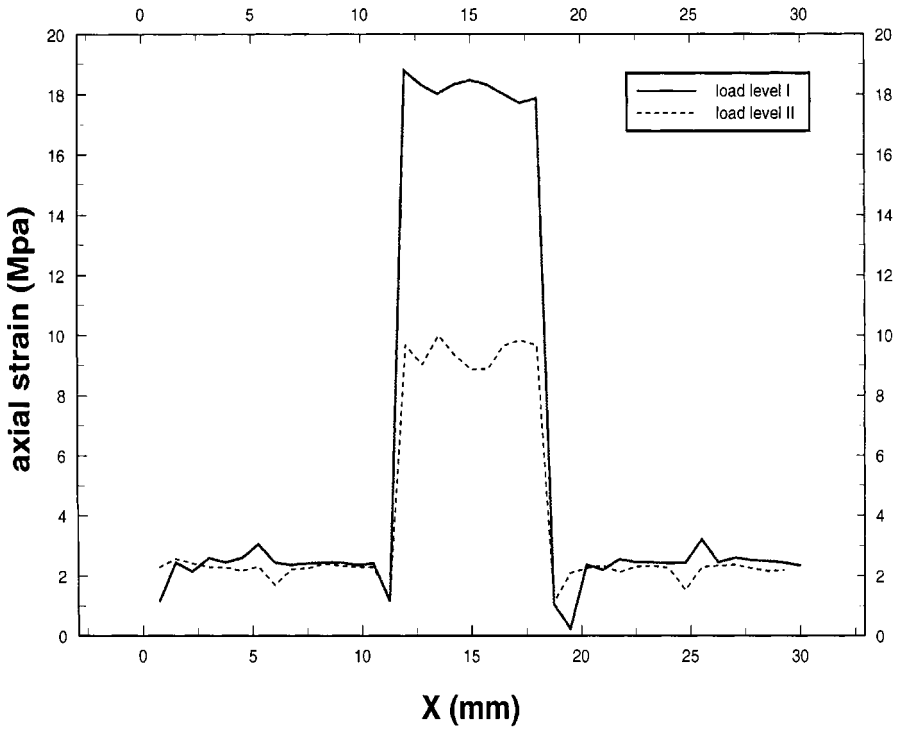

Figure 9. Axial stress in geomembrane

The above solution is developed assuming that the strain in the geomembrane immediately overlying the void is uniform and the strain is zero outside the void area.

For the material properties and geometry used for the numerical simulations with the assumption that the very soft material is equivalent to a void, the calculated constant strain and stress in the geomembrane in response to the load level II are 27 per cent and 28·5 MPa, respectively. The much greater strain predicted by the analytical solution is a consequence of the assumption that the geomembrane does not deform outside the boundaries of the void. In contrast, the numerical simulation indicates that the geomembrane experiences strain well away from the void as shown in Figure 8, consistent with one's expectations. The stress that is predicted by the analytical solution, is closer to the numerical simulation which might be due to the assumed shape of the deformation, or the load p acting on the geomembrane from the overlying soil being similar to that calculated numerically.

5. CONCLUSION

In the paper, a spatial discretization method, that was newly developed for penetration and perforation problems, has been modified for geomechanical problems that involve large deformations and frictional interfaces. The proposed numerical procedure has been compared with analytical solutions, where perfect bonding is assumed without friction along the interface, for the

subsidence of a landfill cover. The results appear to be reasonable in an engineering sense. To quantitatively verify the proposed procedure, well-designed experiments are required to measure the real-time evolution of deformation patterns including friction under external load. When the experimental data become available, advanced constitutive models will be developed to predict the inelastic response including material and interface failure.

APPENDIX I

Consider the equation of motion

$$(\rho\sigma^{\mathrm{s}})\cdot\nabla + \rho\mathbf{B} = \rho\mathbf{A} \tag{25}$$

in which the gradient operator is with respect to the current configuration, σ^{s} denotes the specific stress which is defined to be the Cauchy stress divided by the mass density. The specific body force is **B** and the acceleration is **A**. Apply a weighting function, **W**, to equation (25) and integrate over the current configuration, Ω. After the use of the divergence theorem, the weak form of the equation of motion can be written as

$$\int_{\Omega}\rho\sigma^{\mathrm{s}}:\mathbf{W}\nabla\,\mathrm{d}v + \int\rho\mathbf{W}\cdot\mathbf{B}\,\mathrm{d}v + \int_{\partial\Omega}\mathbf{W}\cdot\mathbf{S}\,\mathrm{d}s = \int_{\Omega}\rho\mathbf{W}\cdot\mathbf{A}\,\mathrm{d}v \tag{26}$$

Introduce the Dirac delta function to discrete mass density

$$\rho = \sum_{q=1}^{N_q}\sum_{p=1}^{N_p} m_{pq}\delta\left[\mathbf{X}-\mathbf{X}_{pq}\right] \tag{27}$$

and nodal basis functions to represent the continuous variables

$$\begin{aligned}\mathbf{W}_{ipq} &= \sum_{i=1}^{N}\mathbf{W}_i N_i(\mathbf{X}_{pq})\\ \mathbf{A}_{ipq} &= \sum_{i=1}^{N}\mathbf{A}_i(t)N_i(\mathbf{X}_{pq})\end{aligned} \tag{28}$$

Thus, the terms in equation (26) can be written as

$$\begin{aligned}\int_{\Omega}\rho\sigma^{\mathrm{s}}:\mathbf{W}\nabla\,\mathrm{d}v &= -\sum_{i=1}^{N}\mathbf{W}_{ipq}\cdot\sum_{q=1}^{N_q}\sum_{p=1}^{N_p} m_{pq}\,\sigma^{\mathrm{s}}_{pq}\cdot\nabla N_i^{\mathrm{T}}(\mathbf{X}_{pq})\\ \int_{\Omega}\rho\mathbf{W}\cdot\mathbf{B}\,\mathrm{d}v &= \sum_{i=1}^{N}\mathbf{W}_{ipq}\cdot\sum_{q=1}^{N_q}\sum_{p=1}^{N_p} m_{pq}\,N_i(\mathbf{X}_{pq})\mathbf{B}_{pq}\\ \int_{\partial\Omega}\mathbf{W}\cdot\mathbf{S}\,\mathrm{d}s &= \sum_{i=1}^{N}\mathbf{W}_{ipq}\cdot\int_{\partial\Omega}N_i(\mathbf{X}_{pq})\mathbf{S}\,\mathrm{d}s\\ \int_{\Omega}\rho\mathbf{W}\cdot\mathbf{A}\,\mathrm{d}v &= \sum_{i=1}^{N}\mathbf{W}_{ipq}\cdot\sum_{q=1}^{N_q}\sum_{p=1}^{N_p} m_{pq}\,N_i^{\mathrm{T}}(X_{pq})N_j(\mathbf{X}_{pq})\mathbf{A}_{jpq}\end{aligned} \tag{29}$$

Denote

$$S_{ipq} = N_i(\mathbf{X}_{pq}) \quad \mathbf{G}^{\mathrm{T}}_{ipq} = \nabla N_i^{\mathrm{T}}(\mathbf{X}_{pq}) \tag{30}$$

and

$$\sum_{q=1}^{N_q}\sum_{p=1}^{N_p} m_{pq}\sigma^{\mathrm{s}}_{pq}\cdot\mathbf{G}^{\mathrm{T}}_{ipq} = \mathbf{F}^{\mathrm{int}}$$

$$\sum_{q=1}^{N_q}\sum_{p=1}^{N_p} m_{pq}S_{ipq}\mathbf{B}_{pq} + \int_{\partial\Omega} S_{ipq}\mathbf{S}\,\mathrm{d}s = \mathbf{F}^{\mathrm{ext}} \tag{31}$$

$$\sum_{q=1}^{N_q}\sum_{p=1}^{N_p} m_{pq}N^{\mathrm{T}}_i(\mathbf{X}_{pq})N_j(\mathbf{X}_{pq}) = m_{ij}$$

with the argument of components of $\mathbf{W}$ are arbitrary except for those points where components of the displacement are prescribed and the understanding that the constraints on the displacement field are invoked, the weak form of the equation of motion yields

$$\sum_{j=1}^{N} m_{ij}\mathbf{A}_j = \mathbf{F}^{\mathrm{int}}_i + \mathbf{F}^{\mathrm{ext}}_i \quad i = 1,2,\ldots,N \tag{32}$$

in which

$$\mathbf{F}^{\mathrm{int}}_i = -\sum_{q=1}^{N_q}\sum_{p=1}^{N_p} m_{pq}(\mathbf{G}^{\mathrm{T}}_{ipq}\sigma^{\mathrm{s}}_{pq})S_{ipq} \tag{33}$$

and

$$m_{ij} = \sum_{q=1}^{N_q}\sum_{p=1}^{N_p} m_{pq}(S^{\mathrm{T}}_{ipq}\,S_{pqj}) \tag{34}$$

APPENDIX II

Strain expression can be directly derived from energy conservation law. Denote the kinematic energy as K and potential energy as P. With the assumption of no thermal effect, the sum of kinematic energy rate and potential energy rate should be zero, i.e.

$$\dot{K} = -\dot{P} \tag{35}$$

Since

$$\dot{K} = \mathbf{V}\cdot\mathbf{F} \tag{36}$$

hence

$$\dot{P} = -\mathbf{V}\cdot\mathbf{F} \tag{37}$$

substitute equation (14) into above equation

$$\begin{aligned}\dot{P} &= -\sum_{i=1}^{N}\mathbf{V}_i\cdot\mathbf{F}_i = \sum_{i=1}^{N}\mathbf{V}_i\cdot\sum_{q=1}^{N_q}\sum_{p=1}^{N_p} m_{pq}(\mathbf{G}^{\mathrm{T}}_{ipq}\sigma^{\mathrm{s}}_{pq})S_{ipq}\\ &= \sum_{q=1}^{N_q}\sum_{p=1}^{N_p} m_{pq}\sigma^{\mathrm{s}}_{pq}:\sum_{i=1}^{N}\mathbf{V}_i\otimes\mathbf{G}^{\mathrm{T}}_{ipq}S_{ipq}\\ &= \sum_{q=1}^{N_q}\sum_{p=1}^{N_p} m_{pq}\sigma^{\mathrm{s}}_{pq}:\varepsilon_{pq}\end{aligned} \tag{38}$$

where

$$\varepsilon_{pq} = \sum_{i=1}^{N} \mathbf{V}_i \otimes \mathbf{G}_{ipq}^{\mathrm{T}} S_{ipq} \tag{39}$$

ACKNOWLEDGEMENTS

We gratefully acknowledge Dr. David Borns at Sandia National Laboratories for his support of this project. The authors are also grateful to the reviewers for discerning comments on this paper.

REFERENCES

1. D. Sulsky, Z. Chen and H. L. Schreyer, 'A particle method for history-dependent materials', *Comput. Meth. Appl. Mech.* **118,** 179–196 (1994).
2. D. Sulsky, S. J. Zhou and H. L. Schreyer, 'Application of a particle-in-cell method to solid mechanics', *Comput. Phys. Commun.* **87,** 236–252 (1995).
3. D. K. Walls and C. Zeiss, 'Municipal landfill biodegradation and settlement', *J. Environ. Engng.*, **121**(3)**,** 214–224 (1995).
4. H. L. Jessberger and K. J. L. Stone, 'Subsidence effects on clay barriers', *Geotechnique*, **41**(2)**,** 185–194 (1991).
5. G. C. Cressman, S. C. Cheng, J. P. Martin and A. S. Bredariol, 'Effects of subsidence distortion on integrity of landfill caps', in *Proc. Environ Geotechnology*, Usmen and Acar (eds), pp. 229–235 (1992).
6. D. E. Daniel, 'Surface barriers: problems, solutions and future needs', in G. W. Gee and N. R. Wing (eds), *In Situ Remediation*: *Scientific Basis for Current and Future Technologies.* 1994, pp. 441–487.
7. I. S. Oweis, 'Sanitary landfill clay caps: do they inhibit leachate generation', *J. Resource Manage. Technol.* **17**(3)**,** 131–137 (1989).
8. N. Gucunski, V. Ganji and M. H. Maher, 'Analysis of settlement of landfill caps by FEM', in H. Fang and H. Inyang, (Eds), *Proc. 3rd Int. Symp. on Environmental Geotechnology*, Technomic Publishing Co., Lancaster, PA, 1996, pp. 485–494.
9. W. L. Murphy and P. A. Gilbert, 'Settlement and cover subsidence of hazardous waste landfills', *US Environmental Protection Agency*, EPA/600/2-85/035, Cincinnati, Ohio, 1985.
10. S. J. Zhou, D. S. Oscar, D. Sulsky and H. L. Schreyer, '*Revised Algorithms for the particle Method Applied to History-Dependent Materials*'. SAND94-UC-705, Sandia National Laboratories, Albuquerque, NM, (1994).
11. F. H. Harlow, 'The Particle-in-Cell Computing Method for Fluid Dynamics in Fundamental Methods in Hydrodynamics', in B. Alder, S. Fernbach and M. Rotenberg (Eds), *Experimental Arithmetic*, *High-Speed Computations and Mathematics*, Academic Press, 1994, pp. 319–345.
12. J. U. Brackbill, D. B. Kothe and H. M. Ruppel, 'FLIP: a low dissipation, particle-in-cell method for fluid flow', *Comput. Phys. Commun.*, **48,** 25–38 (1988).
13. D. Burgess, D. Sulsky and J. U. Brackbill, 'Mass matrix formulation of the FLIP particle-in-cell method', *J. Comput. Phys.* **103,** 1–15 (1992).
14. D. Sulsky and J. U. Brackbill, 'A numerical method for suspension flow', *J. Comput. Phys.*, **96,** 339–368 (1991).
15. D. Sulsky, Z. Zhen and H. L. Schreyer, 'The application of a material—spatial numerical method to penetration', SAND91-7095 UC-705, Sandia National Laboratories, NM 87185, (1991).
16. D. Sulsky, Z. Zhen and H. L. Schreyer, 'A particle method for history-dependent materials', SAND93-7044 UC-705, Sandia National Laboratories, NM 87185, (1993).
17. J. P. Giroud, R. Bonaparte, J. F. Beech and B. A. Gross, 'Design of soil layer—geosynthetic systems overlying voids', *Geotextiles Geomembranes*, **9,** 11–50 (1990).

